International Journal of Computational and Experimental Science and ENgineering (IJCESEN)

Vol. 11-No.4 (2025) pp. 9924-9932
http://www.ijcesen.com

Research Article

ISSN: 2149-9144

Optimization and Simulation of CIGS Thin-Film Solar Cells Using Cd-Free Buffer Layers

Mohammed Boukhalfa[1], Mohammed Mostefaoui[2*], Roumaissa Zenzen[3], Abdelkader Azzeddine Bengharbi[4]

[1]Faculty of Science and Technology, Ziane Achour University, 17000, Djelfa, Algeria.
Email: mohamed.boukhalfa@univ-djelfa.dz - **ORCID:** 0009-0000-5462-698X

[2]Department of Preparatory Classes, Higher School of Saharan Agriculture, Adrar 01000, Algeria,
* **Corresponding Author Email:** m.mostefaoui@urerms.dz - **ORCID:** 0000-0002-9364-1530

[3] Laboratory of mechanical engineering, faculty of sciences and technology, university of jijel
Email: roumaissa.zenzen@univ-jijel.dz - **ORCID:** 0009-0007-8921-9947

[4]Faculty of Technology, Electrical Engineering Department, University of El Oued,Algeria.
Email: bengharbi-aek-azz@univ-eloued.dz - **ORCID:** 0000-0002-3152-6887

Article Info:

DOI: 10.22399/ijcesen.4559
Received: 15 June 2025
Revised: 20 November 2025
Accepted: 01 December 2025

Keywords

CIGS solar cells;
SCAPS
1D simulation;
Buffer layer;
Cd-free materials.

Abstract:

In this work, we propose and evaluate four alternative buffer materials Zn_2SnO_4, ZnS, ZrS_xSe_{1-x}, and SnS_2 as substitutes for CdS in CIGS thin-film solar cells. The numerical simulations were performed using SCAPS-1D to study the effect of absorber (CIGS) and buffer layer thickness on the overall photovoltaic performance. The CIGS absorber thickness was varied from 1 µm to 3.5 µm, while the buffer thickness ranged between 0.01 µm and 0.06 µm. The results show that increasing the absorber thickness enhances Voc, Jsc, and η, with optimal values obtained for 3.0–3.5 µm. The influence of buffer thickness was relatively small, with the best performance achieved for 0.04–0.05 µm. Among the proposed Cd-free buffer layers, ZrS_xSe_{1-x} demonstrated the best performance, achieving results nearly identical to those of the conventional CdS buffer. It exhibited slightly higher Voc and comparable efficiency (η ≈ 22.4%), indicating better band alignment and interface properties.Therefore, ZrS_xSe_{1-x} appears to be a strong environmentally friendly alternative to CdS for high-efficiency CIGS solar cells. The optimized device structure Al/ZnO:Al/ZrS_xSe_{1-x}/CIGS/Mo achieved a maximum simulated efficiency of approximately 22.4%, confirming its potential for next-generation thin-film photovoltaic applications.

1. Introduction

Polycrystalline thin-film solar cells based on $CuInSe_2$ (CIS), $Cu(In,Ga)Se_2$ (CIGS), and CdTe are among the most promising alternatives to conventional wafer-based photovoltaic technologies such as Si and GaAs, owing to their high efficiency, long-term stability, and low manufacturing cost [1] . In particular, CIGS and its sulfur-alloyed derivative $Cu(In,Ga)(S,Se)_2$ (CIGSSe) have attracted significant attention because of their tunable band-gap (1.0–1.7 eV, depending on Ga and S content) and high absorption coefficient (~10^5 cm^{-1}), which enable efficient light harvesting in sub-micrometer absorber layers[2,3]. Furthermore, CIGS thin films can be deposited on diverse substrates such as glass, metal foils, and flexible polymers, allowing the fabrication of lightweight, flexible, and low-cost photovoltaic modules [4]. Current CIGS devices have achieved power conversion efficiencies exceeding 20%, placing them among the highest-performing thin-film solar technologies[5].The standard configuration of a CIGS solar cell consists of a Mo back contact/p-type CIGS absorber/n-type CdS buffer/i-ZnO/ZnO:Al front contact stack [6]. The CdS buffer layer, typically deposited by chemical bath deposition (CBD), plays several critical roles:

- It passivates surface defects and grain boundaries on the CIGS absorber,

- Protects the absorber during sputtering of the ZnO window layer, and

  Optimizes band alignment at the absorber/buffer interface to facilitate carrier separation and collection[7,8].

Despite these advantages, CdS introduces significant drawbacks. From an environmental perspective, cadmium is toxic and carcinogenic, posing serious health and disposal hazards[9,10]. From an optical

- standpoint, its narrow ban-dgap (Eg≈2.4 eV) results in parasitic absorption losses in the blue and ultraviolet regions, limiting the short-wavelength response and thus overall device performance[11]. Consequently, there is growing interest in developing cadmium-free buffer materials that maintain or exceed the performance of CdS while eliminating its environmental impact[12].

In recent years, a number of wide ban-dgap, Cd-free materials including ZnS[13], Zn(O,S)[14], ZnSe[15], and In_2S_3 [16]have been investigated as potential replacements for CdS. These materials exhibit larger band-gaps (2.8–3.7 eV), which reduce optical losses, and can provide favorable conduction band alignment with the CIGS absorber. An optimal buffer layer should create a small positive conduction-band offset that effectively blocks holes while promoting electron transport across the junction[1617].In this work, we propose and evaluate four alternative buffer materials Zn_2SnO_4, ZnS, ZrS_xSe_{1-x}, and SnS_2 as substitutes for CdS in CIGS solar cells. These materials were selected based on their wide band-gaps, chemical stability, and environmental benignity. To assess their suitability, the CIGS solar cell structure was numerically simulated using SCAPS-1D software, which enables detailed modeling of electronic, optical, and interface phenomena in thin-film devices. The simulations aim to analyze the influence of each buffer material on the band alignment, carrier transport, and overall device performance.The ultimate objective of this study is to identify a convenient, non-toxic, and high-performance alternative to CdS that can contribute to the development of sustainable, cadmium-free CIGS solar cells.

2. Materials and methodology

2.1 Numerical simulation of SCAPS-1D

2.1.1. Device Modelling and Material Parameters

The numerical simulations were conducted using SCAPS-1D (Solar Cell Capacitance Simulator), developed by Dr. Marc Burgelman and his team at the Department of Electronics and Information Systems, University of Ghent, Belgium[18,19] . SCAPS-1D is a one-dimensional simulation tool widely employed for modeling thin-film solar cells. It solves the coupled Poisson, continuity, and drift diffusion equations under steady-state conditions to describe charge carrier generation, recombination, and transport within multilayer semiconductor devices[15],[20-28].

$$\frac{1}{q}\frac{dJ_n}{d_x} = r - g\ (for\ electrons) \quad (1)$$

$$\frac{1}{q}\frac{dJ_p}{d_x} = g - r\ (for\ holes) \quad (2)$$

Where g and r are the generation and recombination rates, respectively, and Jn and Jp denote the electron and hole current densities. When both drift and diffusion mechanisms are considered, the current densities can be written as [29-35]:

$$J_P = q\mu_p p\frac{d\emptyset}{dx} - qD_p\frac{d_p}{d_x} \quad (3)$$

$$J_n = q\mu_n n\frac{d\emptyset}{dx} - qD_n\frac{d_n}{d_x} \quad (4)$$

Where μp and μn are the mobilities of holes and electrons, Dp and Dn are their corresponding diffusion coefficients, p and n are the carrier concentrations, q is the elementary charge, and ϕ is the electrostatic potential. The relationship between charge density ρ and electrostatic potential ϕ(x) is governed by the Poisson equation [35-40]:

$$\frac{d^2\emptyset(x)}{dx^2} = -\frac{\rho}{\epsilon} \quad (5)$$

Where:

$$\rho = q(p - n + N_D^+ - N_A^-) \quad (6)$$

Substituting Eq. (6) into Eq. (5) yields:

$$\frac{d^2\emptyset(x)}{dx^2} = -\frac{q}{\varepsilon_0\varepsilon_r}(p - n + N_D^+ - N_A^-) \quad (7)$$

Here, ε_0 and ε_r denote the vacuum and relative permittivities, respectively; N_D^+ and N_A^- represent the concentrations of ionized donors and acceptors. Together, these equations form the physical foundation of the SCAPS-1D model, describing the balance between carrier transport, electrostatic potential distribution, and recombination mechanisms within the simulated solar cell structure.

2.1.2. CIGS solar cell structure

The simulated architecture of the CIGS solar cell consists of a multilayer heterojunction stack arranged as Al / ZnO:Al / Buffer Layer / CIGS / Back Contact, which represents a conventional and well-established thin-film CIGS photovoltaic device configuration. Each layer in this structure fulfills a specific electrical and optical function that is essential for efficient photovoltaic operation.

The Aluminum (Al) layer is employed as the front metallic contact, ensuring efficient extraction and collection of photogenerated charge carriers. Due to its low electrical resistivity and good compatibility with transparent conductive oxides, Al provides minimal series resistance and contributes to reduced ohmic losses in the device.

The Al-doped Zinc Oxide (ZnO:Al) layer serves as the transparent conductive oxide (TCO). This layer plays a dual role by allowing maximum transmission of incident solar radiation into the absorber layer while simultaneously acting as a highly conductive pathway for electron transport toward the external circuit. Aluminum doping significantly enhances the electrical conductivity of ZnO without compromising its high optical transparency in the visible spectrum, thereby improving the overall current collection efficiency.

The buffer layer is a thin n-type semiconductor positioned between the TCO and the absorber. Its primary function is to form a high-quality p–n heterojunction with the p-type CIGS absorber, enabling effective separation of photogenerated electron–hole pairs. Additionally, the buffer layer improves band alignment at the interface, reduces interface defect density, and suppresses carrier recombination losses. Although cadmium sulfide (CdS) is the most widely used buffer material due to its favorable electronic properties and interface quality, alternative cadmium-free buffer layers such as Zn_2SnO_4, ZnS, ZrS_xSe_{1-x}, and SnS_2 have been investigated to address environmental and toxicity concerns while maintaining high device performance.

The CIGS ($Cu(In,Ga)Se_2$) layer acts as the p-type absorber and is the core photoactive region of the solar cell. Owing to its high optical absorption coefficient, a relatively thin CIGS layer is sufficient to absorb the majority of the incident sunlight and generate electron–hole pairs. One of the key advantages of CIGS is its tunable bandgap, which can be adjusted from approximately 1.0 to 1.7 eV by varying the Ga/(In+Ga) ratio. This tunability allows optimization of the absorber for enhanced open-circuit voltage and overall power conversion efficiency.

The back contact layer, typically molybdenum (Mo) or, in the present simulation, platinum (Pt), provides an ohmic contact with the CIGS absorber and ensures efficient hole collection. This layer also offers good mechanical stability and adhesion to the substrate, which is crucial for device reliability and fabrication compatibility.

In this work, the simulated CIGS solar cell structure is defined as Al / ZnO:Al / CdS / CIGS / Pt, as illustrated in Figure 1. All simulations were performed at a standard operating temperature of 300 K, assuming constant carrier mobility across all layers. The electrical and optical material parameters employed in the simulations were extracted from well-established and reliable literature sources, and a detailed summary of these parameters is provided in Table 1.

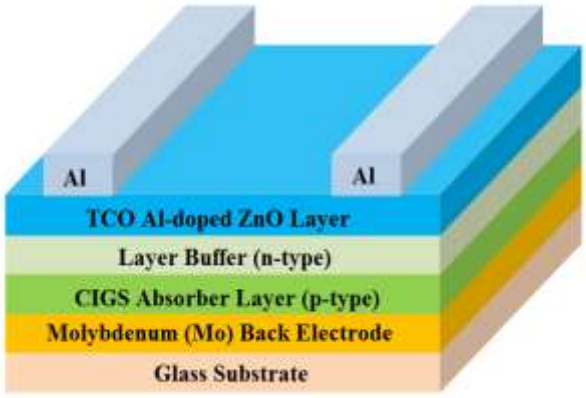

Figure 1. *The general structure of a CIGS thin film solar cell*

Table 1: *Summary of initial parameters set for the simulation of CIGS solar cells [41-49].*

Material properties	**CIGS**	**CdS**	**Zn_2SnO_4**	**ZnS**	**ZnO**	**ZrS_xSe_{2-x}**
Thickness (μm)	Variable	0.1	0.1	0.1	0.1	0.2
Bandgap (Eg)	1.100	2.4	3.3500	3.5	3.3	1.3
Electron affinity χ (eV)	4.500	2.4	4.5000	4.5	4.5	4.7
Dielectric permittivity ε	13.600	10	9.000	10	9.00	16.4
CB density of state	2.200E+18	2.200E+18	2.200E+18	1.500E+18	2.200E+18	2.200E+18
VB density of state	1.800E+19	1.800E+19	1.800E+19	1.800E+18	1.800E+19	1.800E+19

Electron thermal velocity	1.000E + 7	1.000E + 7	1.000E + 7	1.000E + 7	1.000E + 7	1.000E + 7
Hole thermal velocity	1.000E + 7	1.000E + 7	1.000E + 7	1.000E + 7	1.000E + 7	1.000E + 7
Electron mobility	1.00E+2	1.00E+2	3.200E + 1	50	1.00E +2	2300
Hole mobility	2.50E+1	2.50E+1	3.000E + 0	20	2.00E +1	1300
Donor density	1.00E+18	1.00E+18	1.000E + 19	1.00E+18	1.00E+18	1.00E+18
Acceptor density	0.00E+0	0.00E+0	0.000E + 0	0.00E+0	1.00E+5	0.00E+0
Absorption coefficient	SCAPS value	SCAPS value	SCAPS value	SCAPS value	SCAPS value	SCAPS value

3. Result and discussion

3.1 Simulation of CIGS–ZnO(Al) solar cells with Different Buffer Layers :

We initially studied the buffer layer to evaluate its influence on the overall performance of the CIGS ($Cu(In,Ga)Se_2$) thin-film solar cell. The buffer layer plays a crucial role in forming the p–n junction between the CIGS absorber (p-type) and the ZnO:Al window layer (n-type), ensuring efficient charge separation and transport.To investigate this effect, several buffer materials were simulated using the Solar Cell Capacitance Simulator (SCAPS) software, including CdS, ZnS, SnS_2, Zn_2SnO_4, and ZrS_xSe_{2-x} Each material was evaluated under the same device structure (Al/ZnO:Al/Buffer/CIGS/Mo) and standard test conditions (AM 1.5G, 1000 W/m², 300 K).The results showed that all studied structures exhibited high photovoltaic performance, with conversion efficiencies ranging from 21.5% to 22.1%.Among the investigated materials, CdS, SnS_2, and ZrS_xSe_{2-x} provided the best results, reaching efficiencies around 22.1%, due to their favorable band alignment and low interface recombination with the CIGS absorber.The Zn_2SnO_4 and ZnS layers also demonstrated comparable performance ($\eta \approx 21.6\%$) and are considered promising Cd-free alternatives that combine high transparency with good electrical compatibility.These findings confirm that proper buffer layer selection and optimization are essential to achieving high-efficiency, environmentally friendly CIGS-based thin -film solar cells.The simulation results indicate that all CIGS-based solar cells exhibit high efficiencies (21.6–22.1%), with slight variations in the open-circuit voltage (Voc) and short-circuit current density (Jsc).Among the studied buffer materials, CdS, SnS_2, and ZrS_xSe_{2-x} achieved the highest efficiencies (~22.1%), showing optimal band alignment and low interface recombination. Meanwhile, Zn_2SnO_4 and ZnS demonstrate competitive performance and are considered promising cadmium-free alternatives due to their excellent transparency and environmental safety. The J–V characteristics (left) show that all simulated structures exhibit nearly identical diode behavior with high short-circuit current density (Jsc ≈ 38–39 mA/cm²) and open-circuit voltage (Voc ≈ 0.676 V).The QE spectra (right) confirm a strong photoresponse in the wavelength range 400–1000 nm, indicating efficient photon absorption by the CIGS absorber layer. Among the studied buffer materials, CdS, SnS_2, and ZrS_xSe_{2-x} show slightly higher quantum efficiency across the visible spectrum, consistent with their higher conversion efficiencies (~22%).These results confirm the excellent optical and electrical performance of the CIGS–ZnO(Al) structures with different buffer layers.

***Table 2** : Simulated performance parameters of CIGS–ZnO(Al) solar cells with different buffer layers*

Buffer Layer	**Voc (V)**	**Jsc (mA/cm²)**	**FF (%)**	**η (%)**
CdS	0.6764	39.20	83.37	22.10
SnS_2	0.6765	39.19	83.32	22.09
Zn_2SnO_4	0.6758	38.36	83.34	21.60
ZnS	0.6758	38.35	83.33	21.59
ZrS_xSe_{2-x}	0.6769	39.23	83.23	22.10

***Table 3.** Effect of Absorber Layer Thickness on CIGS Solar Cell Performance for CdS (0.05 μm) Buffer.*

Absorber Thickness (μm)	**V_{oc} (V)**	**J_{sc} (mA/cm²)**	**FF (%)**	**η (%)**
1.0	0.6657	37.67	83.00	20.81
1.5	0.6697	38.43	83.14	21.40
2.0	0.6732	38.88	83.27	21.80
2.5	0.6764	39.19	83.37	22.10
3.0	0.6793	39.44	83.44	22.36
3.5	0.6817	39.65	83.54	22.58

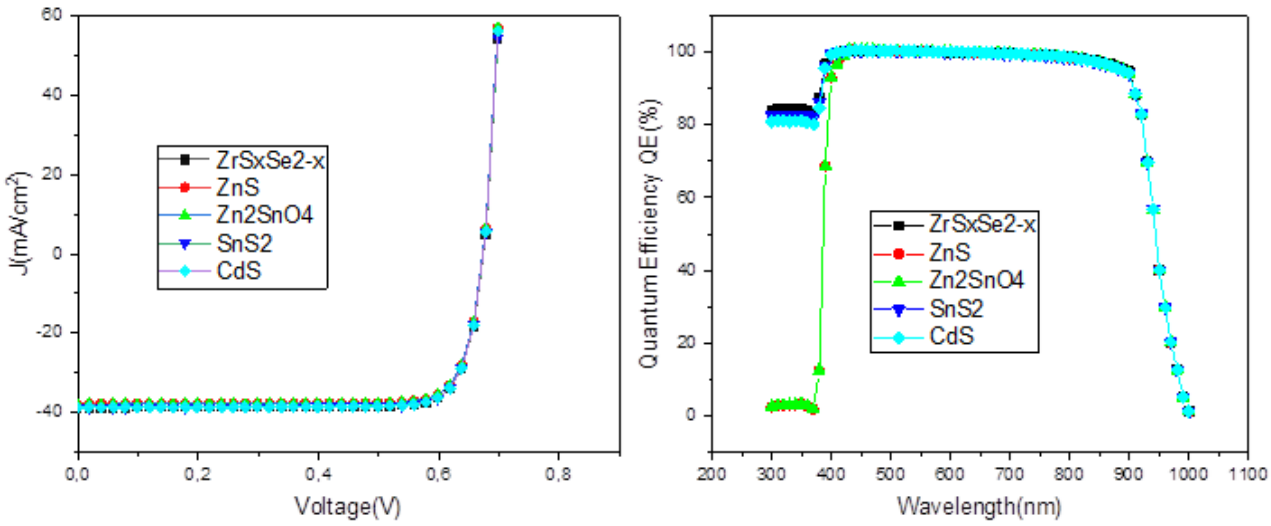

Figure 2. *J–V characteristics and Quantum Efficiency (QE) curves for CIGS solar cells with different buffer layers (CdS, SnS_2, Zn_2SnO_4, ZnS, and ZrS_xSe_{2-x}).*

3.2 Effect of Absorber and Buffer Layer Thickness on CIGS Solar Cell Performance

a. Effect of Absorber Layer Thickness:

To investigate the influence of absorber thickness on device performance, the CIGS absorber layer thickness was varied from 1 µm to 3.5 µm, while the buffer layer (CdS or ZrS_xSe_{2-x}) was kept constant at 0.05 µm.The corresponding photovoltaic parameters open-circuit voltage (Voc), short-circuit current density (Jsc), fill factor (FF), and efficiency (η) are summarized in Table 3 and Table 4.

Table 4. *Effect of Absorber Layer Thickness on CIGS Solar Cell Performance for ZrS_xSe_{2-x} (0.05 µm) Buffer.*

Absorber Layer (µm)	Voc (V)	Jsc (mA/cm²)	FF (%)	η (%)
1	0.666	37.76	82.85	20.85
1.5	0.670	38.48	83.00	21.41
2	0.6737	38.91	83.13	21.80
2.5	0.6769	39.22	83.23	22.10
3	0.6798	39.46	83.31	22.35
3.5	0.6820	39.66	83.43	22.57

As shown in Tables 3 and 4, the photovoltaic parameters (Voc, Jsc, and η) steadily improve as the CIGS absorber thickness increases from 1 µm to 3.5 µm. This improvement is primarily due to enhanced photon absorption and increased carrier generation in thicker absorber layers.However, beyond 3 µm, the improvement becomes marginal since most of the incident light is already absorbed within the layer, and excessive thickness may increase recombination losses.The maximum efficiency (η ≈ 22.6%) is obtained at an absorber thickness of 3.5 µm for both CdS and ZrS_xSe_{2-x} based structures.The solar cell employing ZrS_xSe_{2-x} as a buffer layer exhibits slightly higher Voc and η, suggesting improved band alignment and interface quality compared to CdS. Therefore, an absorber thickness in the range of 3–3.5 µm is considered optimal for achieving high-efficiency CIGS solar cells.

b. Effect of Buffer Layer Thickness

To examine the influence of the buffer layer thickness on the photovoltaic performance of CIGS-based solar cells, the CIGS absorber layer thickness was fixed at 2.5 µm, while the buffer layer thickness was varied between 0.01 µm and 0.06 µm.The corresponding values of open-circuit voltage (Voc), short-circuit current density (Jsc), fill factor (FF), and conversion efficiency (η) are summarized in Table 5 and Table 6 for CdS and ZrS_xSe_{2-x} buffer layers, respectively.As seen in Tables 5 and 6, changing the buffer layer thickness from 0.01 µm to 0.06 µm has only a minor impact on the photovoltaic

Table 5. *Effect of Buffer Layer Thickness on CIGS Solar Cell Performance for CdS Buffer (2.5 µm Absorber)*

Buffer Thickness (µm)	Voc (V)	Jsc (mA/cm²)	FF (%)	η (%)
0.01	0.6764	39.22	83.33	22.11
0.02	0.6764	39.21	83.36	22.11
0.03	0.6764	39.20	83.36	22.11
0.04	0.6764	39.20	83.37	22.10
0.05	0.676	39.19	83.37	22.10
0.06	0.6764	39.19	83.37	22.10

Table 6. *Effect of Buffer Layer Thickness on CIGS Solar Cell Performance for ZrS_xSe_{2-x} Buffer (2.5 µm Absorber).*

Buffer Thickness (µm)	Voc (V)	Jsc (mA/cm²)	FF (%)	η (%)
0.01	0.6767	39.17	83.06	22.02
002	0.6767	39.17	83.08	22.03
0.03	0.6768	39.19	83.12	22.05
0.04	0.6768	39.20	83.16	22.6
0.05	0.6768	39.21	83.20	22.08
0.06	0.6769	39.22	83.23	22.10

parameters. The values of Voc, Jsc, and FF remain nearly constant, while the efficiency (η) shows a small variation around 22.1%.The optimal buffer thickness lies between 0.04 µm and 0.05 µm, where the device achieves stable and maximum efficiency. Thinner buffer layers (<0.02 µm) can cause incomplete junction formation and higher leakage currents, whereas thicker layers (>0.06 µm) tend to absorb part of the incident light, leading to a slight decrease in Jsc. When comparing both materials, the cell with ZrS_xSe_{2-x} buffer demonstrates slightly higher Voc and η values than the CdS-based cell, confirming better band alignment and reduced interface recombination.Therefore, a buffer thickness of 0.04–0.05 µm combined with a 2.5 µm CIGS absorber layer provides the optimal configuration for achieving high-efficiency and environmentally friendly CIGS solar cells.

3.3 Optimal Solar Cell Parameters

The best configuration of the simulated CIGS solar cell corresponds to an absorber thickness of 3.5 µm and a buffer thickness of 0.05 µm. The deduced photovoltaic parameters from the calculated J–V (current–voltage) characteristics for both CdS and ZrS_xSe_{2-x} buffer layers are summarized below.The simulation results show that both buffer materials lead to nearly identical photovoltaic performance under optimized conditions. The CdS-based cell exhibits a slightly higher fill factor (FF), resulting in a marginally higher efficiency of 22.36%. The ZrS_xSe_{2-x}-based cell, however, shows a slightly higher Voc, indicating improved band alignment and potentially lower recombination losses at the interface. Although the efficiency difference is minimal, ZrS_xSe_{2-x} offers an environmentally friendly and cadmium-free alternative to CdS, while maintaining comparable device performance. Therefore, ZrS_xSe_{2-x} can be considered a promising substitute for CdS in high-efficiency CIGS thin-film solar cells.

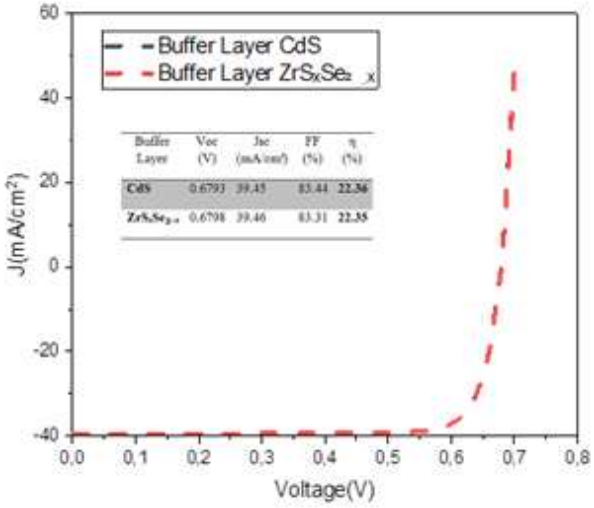

Figure 3*. J–V characteristics of optimized CIGS–ZnO(Al) solar cell structures with different buffer layers.*

4. Conclusion

In this study, the performance of CIGS thin-film solar cells was numerically investigated using the SCAPS-1D simulation program. The effects of both the absorber (CIGS) and buffer (CdS and ZrS_xSe_{2-x}) layer thicknesses on the photovoltaic parameters were systematically analyzed. The results demonstrated that increasing the CIGS absorber thickness from 1 µm to 3.5 µm enhances the device efficiency due to improved photon absorption and carrier generation. However, beyond 3 µm, the improvement becomes marginal as most of the incident light is already absorbed, and thicker layers may induce additional recombination. The optimal absorber thickness was found to be between 3.0 µm and 3.5 µm, where the maximum efficiency of approximately 22.6% was achieved.Similarly, the buffer layer thickness showed only a minor influence on device performance, with optimal results obtained for thicknesses between 0.04 µm and 0.05 µm. Both buffer materials exhibited comparable performance, but the ZrS_xSe_{2-x} layer provided slightly higher Voc and overall stability, highlighting its potential as a Cd-free and environmentally friendly alternative to conventional CdS.In conclusion, the optimized configuration consisting of a CIGS absorber (3.5 µm) and a ZrS_xSe_{2-x} buffer layer (0.05 µm) yields the best balance between light absorption, carrier transport, and junction quality, resulting in an efficiency of about 22.4%. These findings confirm the strong potential of CIGS/ZrS_xSe_{2-x}-based solar cells for the development of high-performance, sustainable photovoltaic devices.

Author Statements:

- **Ethical approval:** The conducted research is not related to either human or animal use.
- **Conflict of interest:** The authors declare that they have no known competing financial interests or personal relationships that could have appeared to influence the work reported in this paper
- **Acknowledgement:** The authors declare that they have nobody or no-company to acknowledge.
- **Author contributions:** The authors declare that they have equal right on this paper.
- **Funding information:** The authors declare that there is no funding to be acknowledged.
- **Data availability statement:** The data that support the findings of this study are available on request from the corresponding author. The data are not publicly available due to privacy or ethical restrictions.

Refrences

[1] A. Romeo, M. Terheggen, D. Abou-Ras, D.L. Bätzner, F.-J. Haug, M. Kälin, D. Rudmann, A.N. Tiwari, Development of thin-film Cu(In,Ga)Se2 and CdTe solar cells, Prog. Photovoltaics Res. Appl. 12 (2004) 93–111. https://doi.org/10.1002/pip.527.

[2] H. Heriche, Z. Rouabah, N. Bouarissa, New ultra thin CIGS structure solar cells using SCAPS simulation program, Int. J. Hydrogen Energy. 42 (2017) 9524–9532. https://doi.org/10.1016/j.ijhydene.2017.02.099.

[3] H.S. Wada T, Hashimoto Y, Nishiwaki S, Satoh T, et al. Negami T, High-efficiency CIGS solar cells with modified CIGS surface, Sol Energy Mater Sol Cells. 67 (2001) 10.

[4] O. Poncelet, R. Kotipalli, B. Vermang, A. Macleod, L.A. Francis, D. Flandre, Optimisation of rear reflectance in ultra-thin CIGS solar cells towards >20% efficiency, Sol. Energy. 146 (2017) 443–452. https://doi.org/10.1016/j.solener.2017.03.001.

[5] H. Arbouz, A. Aissat, J.P. Vilcot, Simulation and optimization of CdS-n/Cu2ZnSnS4 structure for solar cell applications, Int. J. Hydrogen Energy. (2016) 2–7. https://doi.org/10.1016/j.ijhydene.2016.06.185.

[6] B.L. Williams, V. Zardetto, B. Kniknie, M.A. Verheijen, W.M.M. Kessels, M. Creatore, Solar Energy Materials & Solar Cells The competing roles of i-ZnO in Cu (In , Ga) Se 2 solar cells, Sol. Energy Mater. Sol. Cells. 157 (2016) 798–807. https://doi.org/10.1016/j.solmat.2016.07.049.

[7] A.E. Zaghi, M. Buffière, G. Brammertz, M. Batuk, N. Lenaers, B. Kniknie, J. Hadermann, M. Meuris, J. Poortmans, J. Vleugels, Mechanical synthesis of high purity Cu – In – Se alloy nanopowder as precursor for printed CISe thin film solar cells, Adv. POWDER Technol. (2014). https://doi.org/10.1016/j.apt.2014.03.003.

[8] H.W. Schock, R. Noufi, CIGS-based solar cells for the next millennium, Prog. Photovoltaics Res. Appl. 8 (2000) 151–160. https://doi.org/10.1002/(SICI)1099-159X(200001/02)8:1<151::AID-PIP302>3.0.CO;2-Q.

[9] A. Bernard, Cadmium & its adverse effects on human health., Indian J. Med. Res. 128 (2008) 557–64. http://www.ncbi.nlm.nih.gov/pubmed/19106447.

[10] N. Severino, N. Bednar, N. Adamovic, Buffer layer optimization for high efficiency CIGS solar cells, J. Phys. Conf. Ser. 758 (2016). https://doi.org/10.1088/1742-6596/758/1/012016.

[11] N.W. Hoy, L.L. Noto, P.S. Mbule, SCAPS-1D simulation of perovskite solar cells with hydroxyapatite scaffold for lead encapsulation and performance optimization, Next Mater. 9 (2025). https://doi.org/10.1016/j.nxmate.2025.101260.

[12] A. Javed, M.F. Nasir, S. Azam, M.A. Amin, Numerical simulation for a suitable electron transport layer of a lead-free CuInSe2 based perovskite solar cell and PV module, Int. J. Electrochem. Sci. . 20 (2025) 100893. https://doi.org/10.1016/j.ijoes.2024.100893.

[13] M. Mostefaoui, H. Mazari, S. Khelifi, A. Bouraiou, R. Dabou, Simulation of High Efficiency CIGS solar cells with SCAPS-1D software, Energy Procedia. 74 (2015) 736–744. https://doi.org/10.1016/j.egypro.2015.07.809.

[14] S. Merdes, F. Ziem, T. Lavrenko, T. Walter, I. Lauermann, M. Klingsporn, S. Schmidt, F. Hergert, R. Schlatmann, Above 16 % ef fi cient sequentially grown Cu (In , Ga)(Se , S) 2 - based solar cells with atomic layer deposited Zn (O , S) buffers, (2015). https://doi.org/10.1002/pip.

[15] B. Barman, P.K. Kalita, Influence of back surface field layer on enhancing the efficiency of CIGS solar cell, Sol. Energy. 216 (2021) 329–337. https://doi.org/10.1016/j.solener.2021.01.032.

[16] M.A. Ashraf, I. Alam, Numerical simulation of CIGS, CISSe and CZTS-based solar cells with In2S3 as buffer layer and Au as back contact using SCAPS 1D, Eng. Res. Express. 2 (2020). https://doi.org/10.1088/2631-8695/abade6.

[17] A. Chihi, M.F. Boujmil, B. Bessais, Investigation on the Performance of CIGS/TiO 2 Heterojunction Using SCAPS Software for Highly Efficient Solar Cells, J. Electron. Mater. (2017) 1–8. https://doi.org/10.1007/s11664-017-5547-0.

[18] J.M. T, E. K, Numerical Simulation for Optimal Thickness Combination of CdS/ZnS Dual Buffer Layer CuInGaSe2 Solar Cell Using SCAPS 1D, Indian J. Sci. Technol. 12 (2019) 01–06. https://doi.org/10.17485/ijst/2019/v12i45/148395.

[19] M.S. Uddin, R. Hosen, S. Sikder, H. Mamur, M.R.A. Bhuiyan, Photovoltaic performance enhancement of Al/ZnO:Al/i-ZnO/CdS /CIGS/Pt solar cell using SCAPS-1D software, Next Energy. 2 (2024) 100080. https://doi.org/10.1016/j.nxener.2023.100080.

[20] A. Kakade, K.B. Chavan, S. Chaure, N.B. Chaure,

The role of window layers on the simulated performance of CIGS solar cell characteristics using SCAPS-1D, Next Res. 2 (2025) 100334. https://doi.org/10.1016/j.nexres.2025.100334.

[21] A. Rabehi et al., "Current–Voltage, Capacitance–Voltage–Temperature, and DLTS Studies of Ni|6H-SiC Schottky Diode," Semiconductors, vol. 55, no. 4, pp. 446–454, Apr. 2021, doi: 10.1134/S1063782621040138.

[22] F. Mekaret *et al.*, "A comparative study of Schottky barrier heights and charge transport mechanisms in 3C, 4H, and 6H silicon carbide polytypes," *AIP Adv*, vol. 14, no. 11, Nov. 2024, doi: 10.1063/5.0240123.

[23] A. Bekaddour, A. Rabehi, S. Tizi, B. Zebentout, B. Akkal, and Z. Benamara, "Effect of the contact area on the electrical characteristics of the Ti/6H–SiC (n) Schottky diode," *Micro and Nanostructures*, vol. 173, Jan. 2023, doi: 10.1016/j.micrna.2022.207464.

[24] A. Rabehi *et al.*, "Simulation and Experimental Studies of Illumination Effects on the Current Transport of Nitridated GaAs Schottky Diode," *Semiconductors*, vol. 52, no. 16, pp. 1998–2006, Dec. 2018, doi: 10.1134/S106378261816025X.

[25] A. Ziane *et al.*, "Frequency Dependent Capacitance and Conductance–Voltage Characteristics of Nitride GaAs Schottky Diode," *Semiconductors*, vol. 55, no. 1, pp. 51–55, Jan. 2021, doi: 10.1134/S1063782621010206.

[26] A. Rabehi, M. Amrani, Z. Benamara, B. Akkal, and A. H. Kacha, "Electrical and photoelectrical characteristics of Au/GaN/GaAs Schottky diode," *Optik (Stuttg)*, vol. 127, no. 16, pp. 6412–6418, Aug. 2016, doi: 10.1016/j.ijleo.2016.04.113.

[27] A. Ziane *et al.*, "Numerical investigation of G-V measurements of metal - A nitride GaAs junction," *Revista Mexicana de Fisica*, vol. 70, no. 6, pp. 1–7, Nov. 2024, doi: 10.31349/RevMexFis.70.061604.

[28] A. Douara, A. Rabehi, and O. Baitiche, "Impact of AlN interlayer on the electronic and I-V characteristics of In0.17Al0.83N/GaN HEMTs devices," *Revista Mexicana de Fisica*, vol. 69, no. 3, 2023, doi: 10.31349/RevMexFis.69.031602.

[29] A. Douara, A. Rabehi, M. Guermoui, R. Daha, and I. E. Tibermacine, "Impact of AlN Buffer Layer Thickness on Electronic and Electrical Characteristics of In0.17Al0.83N/GaN High-Electron-Mobility Transistor," *Physics of the Solid State*, vol. 66, no. 6, pp. 157–164, Jun. 2024, doi: 10.1134/S1063783424600766.

[30] A. Rabehi *et al.*, "Optimal Estimation of Schottky Diode Parameters Using Advanced Swarm Intelligence Algorithms," *Semiconductors*, vol. 54, no. 11, pp. 1398–1405, Nov. 2020, doi: 10.1134/S1063782620110214.

[31] A. Douara, A. Rabehi, M. Guermoui, R. Daha, and I. E. Tibermacine, "Simulation-based optimization of barrier and spacer layers in InAlN/GaN HEMTs for improved 2DEG density," *Micro and Nanostructures*, vol. 195, Nov. 2024, doi: 10.1016/j.micrna.2024.207950.

[32] A. Rabehi *et al.*, "Accurate parameter estimation of Au/GaN/GaAs schottky diode model using grey wolf optimization," *Revista Mexicana de Fisica*, vol. 70, no. 2, pp. 1–8, 2024, doi: 10.31349/RevMexFis.70.021004.

[33] A. Douara, A. Rabehi, and M. Hamdani, "Effect of Geometrical and Physical parameters of AlGaN/GaN HEMT on the electrical characteristics with AlN spacer layer," 2022.

[34] A. M. Younsi, M. Elbar, and A. Rabehi, "Structural, Electronic, and Optical Properties of Perovskites CaATe3 (A = Zr Or Hf): A Theoretical Investigation," *Semiconductors*, vol. 58, no. 12, pp. 984–992, Dec. 2024, doi: 10.1134/S1063782624601870.

[35] A. Rabehi *et al.*, "Modeling the Abnormal Behavior of the 6H-SiC Schottky Diode Using Lambert W Function," *Journal of Nano- and Electronic Physics*, vol. 14, no. 6, pp. 06032-1-06032–4, 2022, doi: 10.21272/jnep.14(6).06032.

[36] A. Ziane, M. Amrani, Z. Benamara, and A. Rabehi, "Modeling and Simulation of Capacitance–Voltage Characteristics of a Nitride GaAs Schottky Diode," *J Electron Mater*, vol. 47, no. 9, pp. 5283–5290, Sep. 2018, doi: 10.1007/s11664-018-6408-1.

[37] A. Ziane, M. Amrani, A. Rabehi, and Z. Benamara, "Low- and High-Frequency C–V Characteristics of Au/n-GaN/n-GaAs," *Int J Nanosci*, vol. 18, no. 06, p. 1850039, Dec. 2019, doi: 10.1142/S0219581X18500394.

[38] A. Rabehi, H. Helal, D. Zappa, and E. Comini, "Advancements and Prospects of Electronic Nose in Various Applications: A Comprehensive Review," Jun. 01, 2024, *Multidisciplinary Digital Publishing Institute (MDPI)*. doi: 10.3390/app14114506.

[39] A. Douara, A. Rabehi, O. Baitiche, and M. Handami, "Improved electrical characteristics of AlxGa1−xN/GaN High Electron Mobility Transistor by effect of physical and geometrical parameters," *Revista Mexicana de Física*, vol. 69, no. 4 Jul-Aug, Jul. 2023, doi: 10.31349/RevMexFis.69.041001.

[40] M. W. Bouabdelli, F. Rogti, M. Maache, and A. Rabehi, "Performance enhancement of CIGS thin-film solar cell," *Optik (Stuttg)*, vol. 216, Aug. 2020, doi: 10.1016/j.ijleo.2020.164948.

[41] H. Helal, M. Ahrouch, A. Rabehi, D. Zappa, and E. Comini, "Nanostructured Materials for Enhanced Performance of Solid Oxide Fuel Cells: A Comprehensive Review," Apr. 01, 2024, Multidisciplinary Digital Publishing Institute (MDPI). doi: 10.3390/cryst14040306.

[42] H. Helal, Z. Benamara, A. H. Kacha, A. Rabehi, B. Akkal, and M. Amrani, "Electron cyclotron resonance ion source nitridation of Au/n-GaAs schottky diode and current-voltage characterization," in 2017 5th International Conference on Electrical Engineering - Boumerdes (ICEE-B), IEEE, Oct. 2017, pp. 1–6. doi: 10.1109/ICEE-B.2017.8192119.

[43] H. Helal, Z. Benamara, M. Ben Arbia, A. Rabehi, A. C. Chaouche, and H. Maaref, "Electrical behavior of n-GaAs based Schottky diode for different contacts: Temperature dependence of current-voltage," International Journal of Numerical Modelling: Electronic Networks, Devices and Fields, vol. 34, no. 6, Nov. 2021, doi:

10.1002/jnm.2916.

[44] A. Rabehi et al., "Optimal estimation of Schottky diode parameters using a novel optimization algorithm: Equilibrium optimizer," Superlattices Microstruct, vol. 146, p. 106665, Oct. 2020, doi: 10.1016/j.spmi.2020.106665.

[45] H. Helal et al., "A study of current-voltage and capacitance-voltage characteristics of Au/n-GaAs and Au/GaN/n-GaAs Schottky diodes in wide temperature range," International Journal of Numerical Modelling: Electronic Networks, Devices and Fields, vol. 33, no. 4, Jul. 2020, doi: 10.1002/jnm.2714.

[46] F. Bendelala et al., "FDTD Modelling of Nanostructured Hemispherical Plasmonic Light Trapping for Enhanced Ultra-thin GaSb TPV Cell," Semiconductors, vol. 59, no. 4, pp. 404–411, Apr. 2025, doi: 10.1134/S1063782624603029.

[47] H. Helal et al., "Comparative study of ionic bombardment and heat treatment on the electrical behavior of Au/GaN/n-GaAs Schottky diodes," Superlattices Microstruct, vol. 135, p. 106276, Nov. 2019, doi: 10.1016/j.spmi.2019.106276.

[48] H. Helal et al., "A new model of thermionic emission mechanism for non-ideal Schottky contacts and a method of extracting electrical parameters," The European Physical Journal Plus, vol. 135, no. 11, p. 895, Nov. 2020, doi: 10.1140/epjp/s13360-020-00916-5.

[49] H. Helal et al., "Conduction mechanisms in au/0.8 nm–gan/n–gaas schottky contacts in a wide temperature range," Materials, vol. 14, no. 20, Oct. 2021, doi: 10.3390/ma14205909.